NICFD 2024
for Propulsion & Power

Design of experiments to observe liquid-to-vapor expansions exploiting molecularly complex organic fluids

Riccardo Gioia
Politecnico di Milano
riccardo.gioia@polimi.it
Milano, Italy

Alessandro Romei
Politecnico di Milano
alessandro.romei@polimi.it
Milano, Italy

Andrea Spinelli
Politecnico di Milano
andrea.spinelli@polimi.it
Milano, Italy

ABSTRACT

The rising interest in novel two-phase organic Rankine cycles, promising higher efficiency in exploiting low-enthalpy heat sources compared to current single-phase cycles, faces challenges in modeling the flashing process due to insufficient experimental data. To tackle this, the TROVA blowdown wind tunnel will be modified to enable the characterization of flashing processes of molecularly complex fluids. A lumped parameter model is developed to simulate the discharge process of a representative organic fluid, namely hexamethyldisiloxane (MM), and obtain insights into the characteristic times and dimensions compatible with the facility constraints. A preliminary design for a planar converging-diverging nozzle is simulated using computational fluid dynamics, employing a homogeneous equilibrium model. Calculations demonstrate achievable complete vaporization without flow detachment for a useful test duration, corroborating the feasibility of the proposed experimental campaign.

Keywords: liquid-to-dry expansion, flashing flows, organic fluids, design of experiments

1 INTRODUCTION

The necessity to halt climate change through the decarbonization of primary energy consumption has increased interest in the energy efficiency of the industrial sector, which in the EU represents 26 % of primary energy use and is characterized by high losses in the form of waste heat [1]. Nearly half of this rejected heat is low grade, with temperatures below $300-350\,^{\circ}\mathrm{C}$, which can be efficiently exploited using different technologies. One of these is represented by converting waste thermal heat into electric energy employing an organic Rankine cycle (ORC).

A possible further improvement to this mature technology is substituting a single-phase expansion with a two-phase one. Following this idea, the trilateral flashing cycle [2], where the expansion starts from saturated liquid, and the partial evaporative ORC [3], where the expansion begins in the two-phase state, have been proposed. In general, the ability to control the end of evaporation guarantees a better match between the temperatures of the fluid and the heat source, reducing exergy losses and increasing cycle efficiency. Nonetheless, these improvements imply the existence of an expander capable of processing a two-phase flow with an efficiency comparable to that for a single-phase flow [4]. This requirement forces the use of volumetric expanders, thereby limiting the power output below the MW scale.

A possible way to achieve a single-stage two-phase turbine with acceptable efficiency is to leverage the dry characteristic of the saturation curve of molecularly complex fluids, which enables their complete vaporization through an adiabatic expansion in the stator [5], enabling dry operation in the rotor. However, the non-equilibrium effects that characterize this type of expansion must be considered to design a nozzle cascade with acceptable efficiency. This can be achieved by developing an experimentally based model, in analogy with successful attempts for water [6], if experimental data for organic fluids are available. Currently, such data are scarce, except for the experimental campaign carried out by Zhu and Elbel [7, 8]. The expansions studied in the aforementioned campaign begin at a low temperature and end within the saturation dome, due to the shape of the expanded fluid saturation curve, namely R134a. This contrasts with the previously mentioned need to exploit the retrograde shape of the saturation curve to achieve complete vaporization.

To fill this gap, one of the tasks of the POWHER project is to provide reliable experimental data for flashing fluids other than water at thermodynamic conditions relevant to ORC. The selection of relevant thermodynamic conditions is essential because the presence of non-equilibrium is highly dependent on the closeness to the thermodynamic critical point, making it challenging to extrapolate experimental data to different operating conditions. To obtain the necessary data and demonstrate the feasibility of complete vaporization through an adiabatic expansion, the TROVA facility at Politecnico di Milano will be purposely updated. This work highlights the main modifications to the facility and the envisaged expansion processes that will be tested in the upcoming experimental campaign.

2 TROVA MODIFICATIONS FOR TWO-PHASE EXPERIMENTS

The TROVA plant is a blowdown wind tunnel designed to characterize the expansion of organic vapor flows [9]. As shown in Fig. 1, the test rig consists of a high-pressure vessel (HPV) where the fluid is heated and pressurized through an isochoric transformation, a test section where the fluid is expanded, and a low-pressure vessel (LPV) where the fluid is collected and condensed at ambient temperature, ensuring a huge pressure ratio between the two vessels.

Although the current arrangement has been proven successful for the characterization of single-phase organic vapor flow [10, 11], two main modifications are necessary to observe a liquid-to-dry expansion: (i) to extract pressurized liquid from the HPV, a new pipeline connecting the bottom of the HPV to the existing main valve is necessary, (ii) a redesign of the test section, consisting in a planar converging-diverging nozzle. Similarly to the current arrangement, the nozzle will be constructed with two removable inserts to enhance the modularity of the test section.

To accurately identify the intake conditions for validation and repeatability purposes, the adiabatic expansions under study will start from a subcooled liquid state. A possible liquid-to-vapor expansion is shown in Fig. 2, considering hexamethyldisiloxane (MM) as the working fluid. Due to budget constraints, expansions starting within the saturation dome are excluded, as they would have required detailed characterizations of the initial two-phase flows in terms of vapor quality and flow regime (e.g., annular, bubbly, stratified, etc.).

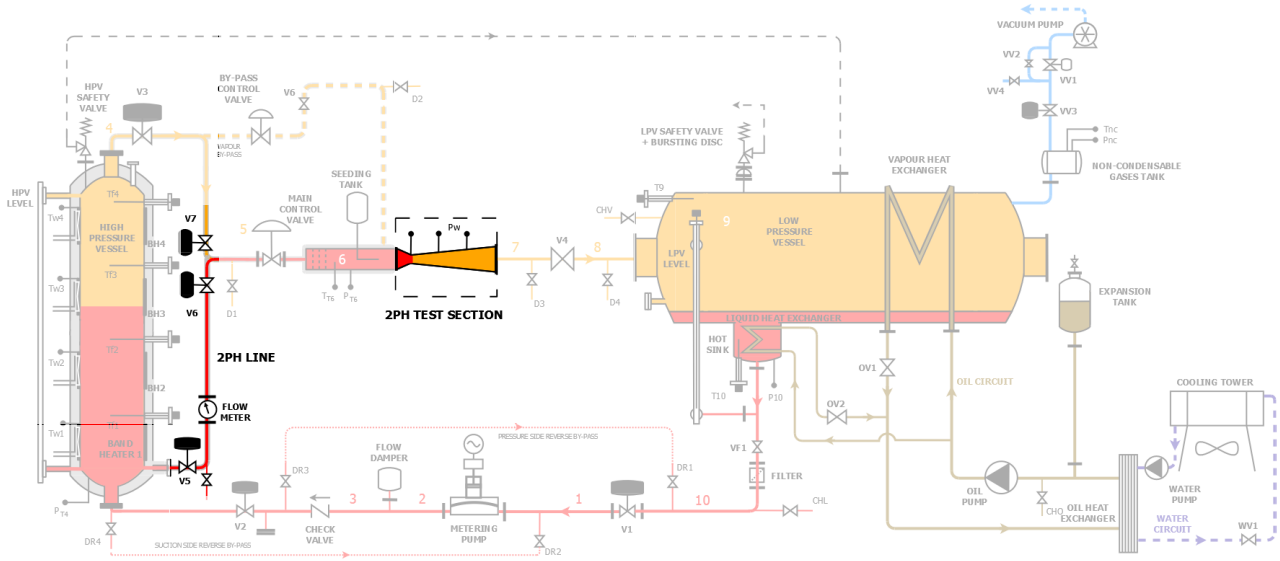

Figure 1: *Schematic of the TROVA test rig with the main modifications highlighted.*

3 LUMPED PARAMETER MODEL OF THE DISCHARGE PROCESS AND NOZZLE SIZING

To gain a first insight into suitable boundary conditions to achieve complete vaporization and estimates of the nozzle gross dimensions, a lumped parameter model has been developed and detailed in the next sections.

3.1 Discharge model with no losses

The discharge process is modeled by solving continuity and energy equations using a forward time-marching method:

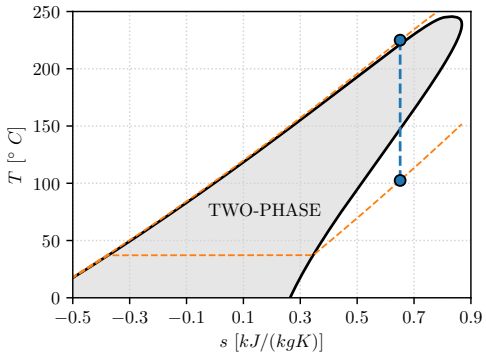

Figure 2: *Example of an isentropic liquid-to-dry expansion in the temperature-specific entropy (T, s) diagram for MM. Inlet conditions are* $T = 225$ °C *and* $P = 30$ bar*, while outlet pressure is* $P = 0.1$ bar.

$$\frac{dm_{HPV}}{dt} = -\dot{m}_{out} \implies m_{HPV}^{(i+1)} = m_{HPV}^{(i)} - \dot{m}_{out}^{(i)} \Delta t \tag{1}$$

$$\frac{dU_{HPV}}{dt} = -\dot{m}_{out} h_{out}^{t} \implies u_{HPV}^{(i+1)} = u_{HPV}^{(i)} - \frac{\dot{m}_{out}^{(i)} \mathscr{H}\left(\rho_{HPV}^{(i)}, u_{HPV}^{(i)}\right)}{m_{HPV}^{(i)}} \Delta t \tag{2}$$

where (i) represents the time discretization and $\mathscr{H}$ is the function, evaluated using CoolProp [12], that correlates the specific enthalpy with the HPV thermodynamic state. The selection of (ρ, u) as an independent thermodynamic pair enables the complete definition of the flow thermodynamic state even in the presence of a two-phase flow. For a given A_{th}, $\dot{m}_{out}$ is computed by maximizing the mass flux ρV under the assumption of isentropic and adiabatic flow. To account for the increase in $\dot{m}_{out}$ due to potential non-equilibrium, which delays the formation of vapor resulting in a higher density (closer to that of a liquid), a corrective factor κ is employed, with a value ranging between 1 (complete equilibrium) and 1.5 (non-equilibrium).

The model also estimates $A_{out,n}$ necessary to reach the prescribed $P_{out,n}$, which is set to one-fourth of the saturated vapor pressure ($P_{s,v}$) obtained through an isentropic expansion from the initial total conditions. Selecting $P_{out,n}$ lower than $P_{s,v}$ ensures a margin for complete vaporization in the presence of non-equilibrium effects.

3.2 Discharge model with losses

To account for the effects of the pressure drop in the line connecting the HPV with the test section, a lumped parameter loss model is developed. As a result, the thermodynamic state that appears in the system of equations (1)-(2) differs from the one in the HPV. The line upstream of the test section is divided into different elements corresponding to each hydraulic device. The pressure loss of the element j is computed using Eq. (3), where the value of the loss coefficient $\xi^{(j)}$ is determined according to Idel'chik [13] and $V^{(j)}$ is the absolute reference velocity for the element j. After each element, ρ is updated to consider the decrease in P due to P_{loss} and the increase in internal energy due to viscous loss. Thus, $\rho^{(j-1)}$ in Eq. (3) represents the ρ computed after the previous element.

$$P_{loss}^{(j)} = \frac{1}{2} \xi^{(j)} \rho^{(j-1)} V^{(j)2} \tag{3}$$

In the model, the distributed losses along the pipes are considered together with the local losses related to the entrance, diffusers, elbows, valves, Coriolis flow meter, porous breakwater, disk breakwater, and convergent nozzle. Moreover:

- The local pressure drop inside the ball valves, i.e. V5 and V6 in Fig. 1, is neglected because they are fully open in steady conditions, meaning that a ball valve is comparable to a straight pipe from the point of view of the loss model. The manufacturer has confirmed the validity of this assumption.

- The $P_{loss,\,CFM}$, which is the loss associated with the Coriolis flow meter (in Section 5 the presence of the flow meter is discussed in more detail) is treated as a parabolic function of $\dot{m}$. The analytical function is determined by interpolating the data provided by the manufacturer.

3.3 Analysis of the discharge process simulation

The conditions in the HPV at $t = 0$ s are $T_{HPV} = 225$ °C and $P_{HPV} = 30$ bar. The fluid is hexamethyldisiloxane (MM). The time window for the discharge process ranges between 0 and 20 s. The equations (1)-(2) are discretized with a time step of $\Delta t = 0.1$ s. Both inviscid and viscous cases are considered. The calculations are based on the assumption of an equivalent throat diameter of $D_{th} = 8$ mm. The worst-case scenario with $\kappa = 1.5$ is discussed, leading to a faster discharge process because of non-equilibrium effects.

The temporal evolution of P_{HPV} and $P_{s,l}$ is shown in Fig. 3a. Note that $P_{s,l} = \mathscr{P}(T_{in,n}, X = 0)$, where $\mathscr{P}$ is the function, evaluated using CoolProp, that correlates the saturated liquid pressure with the temperature at the nozzle inlet. The difference between these two pressures represents the subcooling margin from the saturated conditions. The acquisition starts at $t = 5$ s (black line) to exclude the initial transient effects of the fast valve opening, while the end time is reached when the phase change onset in the upstream pipeline (i.e., two-phase flows at the nozzle inlet). As P_{HPV} decreases during the emptying process, the HPV tends towards a vapor-liquid equilibrium. When this condition is reached, the subcooling is only ensured by the head of the liquid. This pressure margin from saturation is insufficient to preserve the subcooled liquid condition at the nozzle inlet. In addition, P_{HPV} and $\dot{m}$ exhibit a clear relation: the decrease of P_{HPV} is mainly due to the emptying of the HPV with a rate proportional to $\dot{m}$. At the same time, as P_{HPV} reduces, $\dot{m}$ also decreases, reaching a minimum and near-constant value when vapor-liquid equilibrium is established in the plenum. Under this light, the first derivative of P_{HPV} decreases until it flattens when flashing occurs at the nozzle inlet.

The end time for the inviscid and viscous cases is almost the same (13.0 s vs 13.2 s), guaranteeing an acquisition length of about 8 s. At $t = 0$ s, the presence of a pressure drop related to the effect of viscous forces reduces both $P_{in,n}$ and $\dot{m}$, thus slowing down the HPV emptying compared to the inviscid one, as demonstrated by the higher value of the P_{HPV} in Fig. 3a. Nonetheless, the variations are marginal, and the effects of losses can be regarded as negligible on the test duration.

The corresponding values of $y_{out,n}$ for the viscous case at various b/y_{th} are reported in Fig. 3b. The initial idea is to design a nozzle with the value of $y_{out,n}$ computed at $t = 5$ s, ensuring that a pressure lower than the prescribed $P_{out,n}$ would always be reached during the data acquisition. Nevertheless, this is not possible, except for the geometry with $b/y_{th} = 5$, because of a constructive constraint that limits the maximum $y_{out,n}$ to the value of the internal diameter of an ASME schedule 80 pipe with a diameter of 4" (indicated by the horizontal dashed black line in Fig. 3b). However, $b/y_{th} = 5$ is not acceptable because the obtained y_{th} would be too small ($y_{th} = 3.1$ mm). In an effort to increase the throat dimension, $b/y_{th} = 3$ is

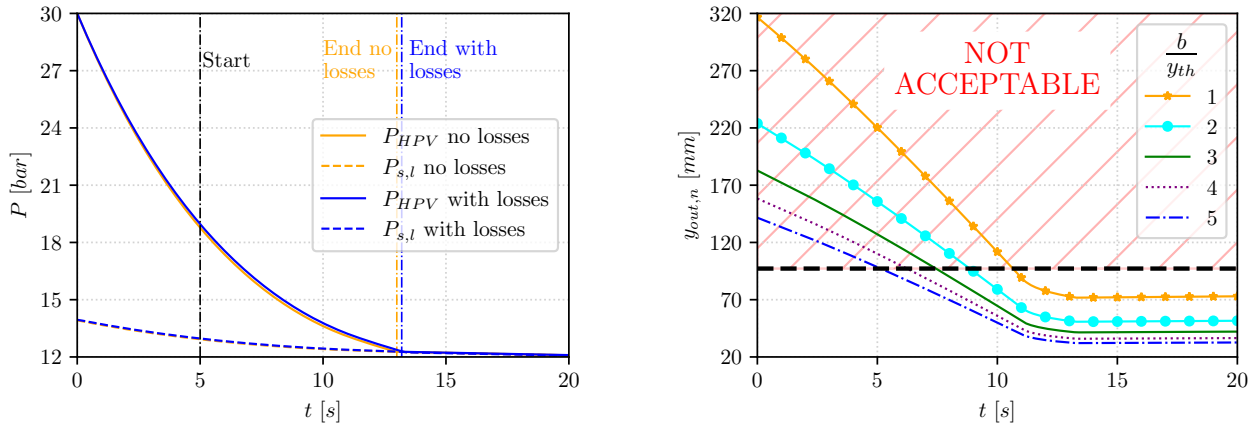

(a) (b)

Figure 3: *(a) Variation of P_{HPV} and $P_{s,l}$ at the nozzle inlet during the studied time window. (b) Variation of $y_{out,n}$ during the studied time window. The dotted black line in (b) indicates the maximum allowable $y_{out,n}$, limited by constructive constraints.*

selected, corresponding to a nozzle designed with the proper $y_{out,n}$ for $t = 7.5$ s and featuring an y_{th}, equal to 4.1 mm.

4 CFD ANALYSIS

Two-dimensional and steady CFD simulations with homogeneous equilibrium model (HEM) are performed in Ansys-Fluent® to understand the flow field in a converging-diverging nozzle designed following the previous section. The thermodynamic properties are provided through look-up tables, using as primitive state variables (P,h). A more detailed explanation of the flow model used can be found in Romei et al. [14]. In this context, the use of HEM is justified by the selected expansion starting point, which is close to the critical point, where the non-equilibrium effects are expected to be negligible. Further analyses with more refined non-equilibrium models are already underway.

The simulated nozzle is designed using two Bézier curves with four control points each, one curve for the convergent part and the other for the divergent part. The passage areas at the throat and outlet are computed solving the continuity equation under the assumption of isentropic adiabatic flow conditions. Zero slopes are imposed at all two sections. The control points for the diverging sections are positioned to ensure a gradual decrease in slope going toward the outlet. Lastly, due to a constructive constraint on the test section maximum length, the total nozzle length is equal to 188 mm. A longer diverging part, with a length of 136 mm, is selected by sacrificing the converging one because of the large area ratio between the outlet section and the throat, equal to 21.7.

The nozzle is designed with the values P_{HPV}, T_{HPV}, and $P_{out,n}$ computed at $t = 7$ s with the lumped parameter model without losses. The same assumptions of Section 3.3 are used, except for $\kappa = 1$ to comply with the equilibrium assumption of the employed flow model.

To better explain why different values of κ have been employed in the lumped parameter model and the nozzle design for the CFD simulations, a more in-depth explanation of the effects related to the variation of κ is necessary. As explained by White [5], the dramatic decrease in the speed of sound related to the phase change causes supersonic flow in the vicinity of the geometrical throat, meaning that the actual $\dot{m}$ is equal to the choked one independently of non-equilibrium effects. However, delayed vapor formation decreases the actual X from its value in equilibrium, thereby increasing the mixture density and, correspondingly, the choked $\dot{m}$.

The nozzle geometry is simulated with three different inlet and outlet boundary conditions. The idea is to observe how a nozzle designed with the total pressure and temperature computed at $t = 7$ s behaves in off-design conditions, namely $t = 5$ s and $t = 9$ s. In all three CFD simulations only half of the passage area, discretized with a structured mesh made up of about 215 000 quadrilateral elements, is simulated. Turbulence is modeled using the $\kappa-\omega$ *SST* model, assuring $y^+ < 1$ along the profile. All equations are solved using second-order methods. At the inlet, the total pressure, total enthalpy, turbulence intensity, and hydraulic diameter are assigned, while only the static pressure is assigned at the outlet. Finally, symmetry and smooth-wall boundary conditions are assigned along the axis of symmetry and nozzle profile, respectively.

The Mach contour for the $t = 7$ s case, as illustrated in Fig. 4, indicates the absence of flow detachment, which may occur due to the significant area ratio. In the same contour, two discontinuities in the Mach number can be observed: one near the geometrical throat and another inside the divergent part, corresponding to the beginning and end of the vaporization, respectively. As widely described in the literature [15], the speed of sound computed employing the HEM is characterized by the presence of discontinuities in correspondence with saturation conditions. Another consequence of the HEM is that the two-phase speed of sound at equilibrium increases along isentropic expansions, motivating the maximum M right after the throat. Weak shocks are visible in the first half of the divergent nozzle (as shown in the zoom of Fig. 4), but they can arguably be eliminated with a more refined nozzle design via shape optimization. Finally, complete vaporization is achieved at around half of the divergent, demonstrating an adequate margin to comply with potential vapor formation delay.

Figure 5 reports the non-dimensional pressure and vapor quality trends along the nozzle axis for the three operating conditions. The shocks are merely shifted by the change in the inlet total conditions without any amplification in the shock strength. Optimizing the nozzle profile to eliminate the shock under design conditions could possibly eliminate the shock train in other operating conditions as well. The primary difference in the behavior of $P/P_{in,n}$ among the three cases is located in the first half of the divergent part. This difference can be attributed to similar P_{th} values and, consequently, the need for greater expansion with higher inlet total conditions.

Furthermore, the vaporization end occurs sooner as t increases, as shown in Fig. 5b, because the total-to-static expansion ratio to reach complete vaporization reduces. However, the worst-case scenario ($t = 5$ s) still foresees a complete vaporization at $z/L = 0.58$. Such early vaporization results from the choice to design the nozzle for $P_{out,n} = 0.25\,P_{s,v}$ as a

safety measure to account non-equilibrium effects.

As expected, $\dot{m}$ decreases with the decrease of the total inlet conditions, see Tab. 1. This comparison also demonstrates that the lumped parameter model presented in Section 3 can predict the actual $\dot{m}$ with acceptable accuracy, although with an overestimation of around $5.6 - 5.7$ %. This overestimation can be attributed to two-dimensional effects in the vicinity of the throat.

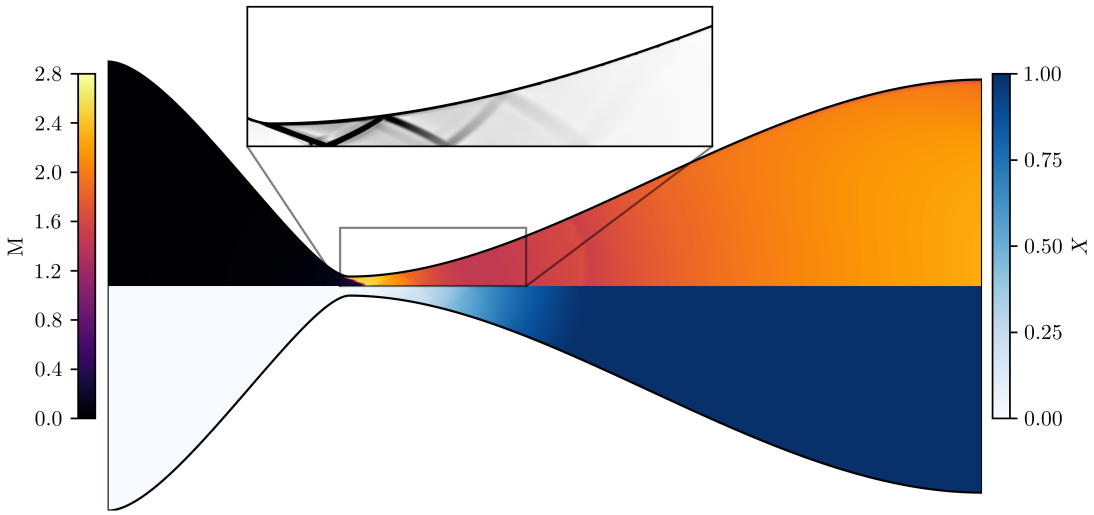

Figure 4: *M (above), X (below), and density gradient (zoom) contours for the* $t = 7$ s *case.*

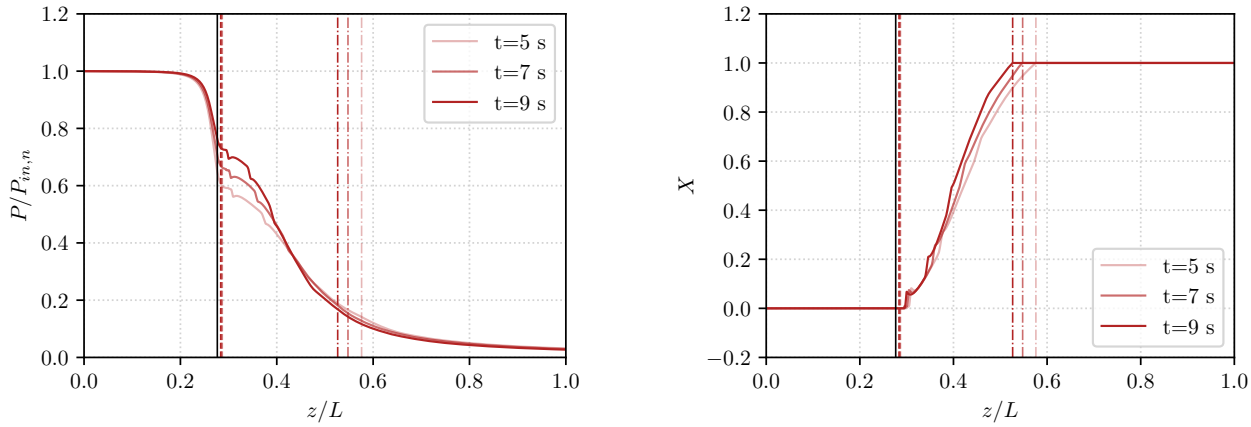

(a) (b)

Figure 5: *(a) Variation of nondimensional P along the axis of symmetry, and (b) variation of X along the axis of symmetry. The black solid line indicates the position of the geometrical throat, the dashed line indicates the start of the phase change, while the dash-dotted line indicates the end of the vaporization.*

Table 1: *Choked mass flow rate by the lumped parameter model and the CFD simulation for the three simulated cases.*

t [s]	$\dot{m}_{LP}$ [kg/s]	$\dot{m}_{CFD}$ [kg/s]	Relative difference [%]
5.0	1.44	1.36	5.75
7.0	1.25	1.18	5.75
9.0	1.07	1.01	5.61

5 RESEARCH QUESTION AND REQUIRED INSTRUMENTATION

During the experimental campaign, three main research questions will be addressed as follows:

1. The demonstration of complete vaporization through adiabatic expansion will be accomplished via qualitative optical visualization. High-speed digital imaging and shadowgraphy have been selected as optical techniques due to their proven ability to visualize two-phase flows [16, 17]. Additionally, during post-processing, if the grey contrast across the two-phase interface is sufficient, the locations of incipient and complete vaporization will be determined. Two optical accesses, one on each side of the test section (Fig. 6), are necessary to perform this type of measurement.

2. The experimental data required for the development and validation of flashing flow models will be obtained by measuring the pressure at the nozzle walls using pressure taps drilled into the inserts, see Fig. 6. These taps are asymmetrically positioned, except for two on each side, allowing for increased spatial resolution while also verifying the symmetry of the flow. Additionally, all tap positions are optically accessible, enabling the assessment of the actual flow state at each corresponding location.

3. A quantitative characterization of potential non-equilibrium between phases may be achieved by comparing $\dot{m}_{CFM}$, measured by a Coriolis flow meter mounted along the line upstream of the test section, with $\dot{m}_{HEM}$, computed numerically under the assumption of thermodynamic equilibrium and homogeneous flows. This comparison is justified by observing that the expected flow in the nozzle is supersonic and choked [5] and that delayed vapor formation is associated with a higher value of $\dot{m}$ than expected under equilibrium conditions.

Although the effectiveness of the employed techniques is widely proven in the literature, some criticalities can be identified for both the selected optical techniques and the Coriolis flow meter. Specifically:

- Regarding high-speed digital imaging and shadowgraphy, their inability to provide a complete three-dimensional reconstruction of the flow can lead to misjudgments of the actual void fraction [17]. This limitation can occur, for example, in the case of annular flow: the presence of vapor near the walls renders the flow opaque, and consequently, the liquid core cannot be detected by the camera.
- The indirect characterization of non-equilibrium through the comparison of $\dot{m}_{CFM}$ with $\dot{m}_{HEM}$ presents three conceptual problems that may possibly limit the envisaged characterization:
    1. The start of the flashing must occur before the geometrical throat to establish a meaningful connection between the choking $\dot{m}$ and the level of non-equilibrium.
    2. The difference between $\dot{m}_{CFM}$ and $\dot{m}_{HEM}$ can be attributed to factors other than the presence or absence of equilibrium, such as turbulence modeling, boundary layers, and flow non-uniformity, potentially leading to an overestimation of the actual degree of non-equilibrium.
    3. The characterization is valid only in the vicinity of the throat, while no information can be derived about how the non-equilibrium evolves through the expansion.

Despite the discussed limitations, the proposed experiment is considered a reasonable starting point for the characterization of organic fluid flashing flows.

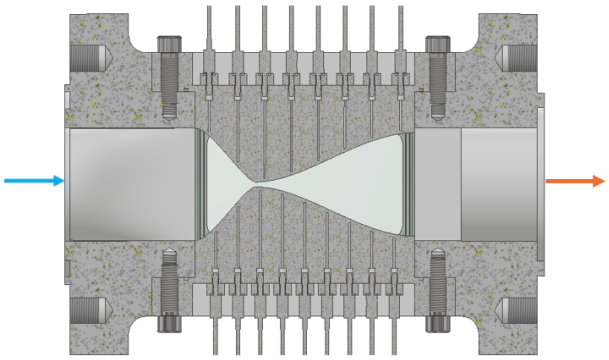

Figure 6: *Preliminary design of the new test section with the simulated profile.*

6 CONCLUSIONS AND FUTURE WORKS

This paper outlines the design of an experimental campaign in the TROVA facility to characterize liquid-to-vapor expansions of organic fluids. The nozzle gross dimension and operating conditions are derived from modeling the discharge process with a lumped parameter approach. These conditions are then utilized to set the boundary conditions for CFD simulations of a preliminary nozzle design, employing a homogeneous equilibrium model. The CFD results demonstrate that complete vaporization without flow separation is achievable over a sufficiently extended period. These preliminary results confirm the feasibility of the planned experimental campaign and will be used to finalize the design of experiments.

The selected measurement techniques and instrumentation for characterizing the liquid-to-dry expansion of an organic dry fluid are also illustrated. The planned characterization includes assessing the actual flow state during the expansion using high-speed digital imaging and shadowgraphy, acquiring useful data for developing and validating flashing flow models by measuring the pressure at the nozzle walls, and quantitatively evaluating the degree of non-equilibrium in the vicinity of the throat by measuring the actual $\dot{m}$.

Acknowledgment

We acknowledge financial support under the National Recovery and Resilience Plan (NRRP), Mission 4, Component 2, Investment 1.1, Call for tender No. 1409 published on 14.9.2022 by the Italian Ministry of University and Research (MUR), funded by the European Union – NextGenerationEU– Project Title: Partial evaporation ORC systems for industrial waste heat recovery - POWHER (P2022MEYKS_002) – CUP D53D23018390001 - Grant Assignment Decree No. 1385 adopted on 01/09/2023 by the Italian Ministry of Ministry of University and Research (MUR).

References

[1] R. Agathokleous, G. Bianchi, G. Panayiotou, L. Arestia, M. C. Argyrou, G. S. Georgiou, S. A. Tassou, H. Jouhara, S. A. Kalogirou, G. A. Florides, and P. Christodoulides, "Waste heat recovery in the eu industry and proposed new technologies," *Energy Procedia*, vol. 161, pp. 489–496, 3 2019.

[2] D. G. Elliot, "Theory and tests of two-phase turbines," *Jet Propulsion Laboratory Publication 81-105, Pasadena CA*, 1982.

[3] S. Daniarta, P. Kolasiński, and A. R. Imre, "Thermodynamic efficiency of trilateral flash cycle, organic rankine cycle and partially evaporated organic rankine cycle," *Energy Conversion and Management*, vol. 249, p. 114731, 12 2021.

[4] M. T. White, "Cycle and turbine optimisation for an orc operating with two-phase expansion," *Applied Thermal Engineering*, vol. 192, p. 116852, 6 2021.

[5] M. T. White, "Investigating the wet-to-dry expansion of organic fluids for power generation," *International Journal of Heat and Mass Transfer*, vol. 192, p. 122921, 8 2022.

[6] M. D. Lorenzo, P. Lafon, J.-M. Seynhaeve, and Y. Bartosiewicz, "Benchmark of delayed equilibrium model (dem) and classic two-phase critical flow models against experimental data," *International Journal of Multiphase Flow*, vol. 92, pp. 112–130, 6 2017.

[7] J. Zhu and S. Elbel, "Experimental investigation of a novel expansion device control mechanism: Vortex control of initially subcooled flashing r134a flow expanded through convergent-divergent nozzles," *International Journal of Refrigeration*, vol. 85, pp. 167–183, 1 2018.

[8] J. Zhu and S. Elbel, "Measurement of static pressure profiles of vortex flashing r134a flow expanded through convergent–divergent nozzles," *International Journal of Refrigeration*, vol. 108, pp. 258–270, 12 2019.

[9] A. Spinelli, M. Pini, V. Dossena, P. Gaetani, and F. Casella, "Design, simulation, and construction of a test rig for organic vapors," *Journal of Engineering for Gas Turbines and Power*, vol. 135, 4 2013.

[10] A. Spinelli, G. Cammi, S. Gallarini, M. Zocca, F. Cozzi, P. Gaetani, V. Dossena, and A. Guardone, "Experimental evidence of non-ideal compressible effects in expanding flow of a high molecular complexity vapor," *Experiments in Fluids*, vol. 59, pp. 1–16, 8 2018.

[11] S. Gallarini, F. Cozzi, A. Spinelli, and A. Guardone, "Direct velocity measurements in high-temperature non-ideal vapor flows," *Experiments in Fluids*, vol. 62, p. 199, 10 2021.

[12] I. H. Bell, J. Wronski, S. Quoilin, and V. Lemort, "Pure and pseudo-pure fluid thermophysical property evaluation and the open-source thermophysical property library coolprop," *Industrial & Engineering Chemistry Research*, vol. 53, pp. 2498–2508, 2014.

[13] I. E. Idel'chik and A. S. Ginevskii, *Handbook of hydraulic resistance*. Begell House, 2007.

[14] A. Romei, P. Gaetani, and G. Persico, "Computational fluid-dynamic investigation of a centrifugal compressor with inlet guide vanes for supercritical carbon dioxide power systems," *Energy*, vol. 255, p. 124469, 9 2022.

[15] M. D. Lorenzo, "Modelling and numerical simulation of metastable two-phase flows," 5 2018.

[16] P. F. Dunn, F. O. Thomas, M. P. Davis, and I. E. Dorofeeva, "Experimental characterization of aviation-fuel cavitation," *Physics of Fluids*, vol. 22, 11 2010.

[17] A. Dash, S. Jahangir, and C. Poelma, "Direct comparison of shadowgraphy and x-ray imaging for void fraction determination," *Measurement Science and Technology*, vol. 29, p. 125303, 12 2018.

NOMENCLATURE

Roman symbols

Δt	time interval [s]
$\dot{m}$	Mass flow rate [kg/s]
A	Passage area [mm^2]
b	Nozzle thickness [mm]
D	Diameter [mm]
h	Specific enthalpy [J/kg]
M	Mach Number
m	Mass [kg]
P	Pressure, [bar]
$P/P_{in,n}$	Nondimensional pressure
T	Temperature, [°C]
t	time [s]
U	Internal energy, [J]
u	Specific internal energy, [J/kg]
V	velocity [m/s]
y	Nozzle height [mm]
z/L	Nondimensional axial coordinate

Greek symbols

κ	Corrective factor for the non-equilibrium effects on $\dot{m}$
ρ	Density [kg/m^3]
X	Vapor quality

Non-dimensional numbers

ξ	Loss coefficient

Sub- and super-indices

(i)	Variable computed at the (i) timeframe
(j)	Variable computed referring to the (j) element
in, n	Variable computed at the nozzle inlet
$loss$	Viscous loss for a given element
out	Variable computed at the HPV outlet
out, n	Variable computed at the nozzle outlet
s, l	Condition at saturated liquid state
s, v	Condition at saturated vapor state
t	Total condition
th	Variable computed at the geometrical throat
CFD	Variable computed with the CFD
CFM	Variable measured by the Coriolis flow meter
HEM	Variable computed with a HEM
HPV	Variable computed in the HPV
LP	Variable computed with the lumped parameter model